INFECTION AND IMMUNITY, Mar. 2007, p. 1154–1166 Vol. 75, No. 3
0019-9567/07/$08.00+0 doi:10.1128/IAI.00943-06

Virally Activated CD8 T Cells Home to *Mycobacterium bovis* BCG-Induced Granulomas but Enhance Antimycobacterial Protection Only in Immunodeficient Mice▽

Laura H. Hogan,[1] Dominic O. Co,[1]† Jozsef Karman,[1]‡ Erika Heninger,[1] M. Suresh,[2] and Matyas Sandor[1]*

Department of Pathology and Laboratory Medicine, University of Wisconsin School of Medicine and Public Health, Madison, Wisconsin 53706,[1] and Department of Pathobiological Sciences, School of Veterinary Medicine, University of Wisconsin, Madison, Wisconsin 53706[2]

Received 13 June 2006/Returned for modification 9 August 2006/Accepted 10 December 2006

The effect of secondary infections on CD4 T-cell-regulated chronic granulomatous inflammation is not well understood. Here, we have investigated the effect of an acute viral infection on the cellular composition and bacterial protection in *Mycobacterium bovis* strain bacille Calmette-Guérin (BCG)-induced granulomas using an immunocompetent and a partially immunodeficient murine model. Acute lymphocytic choriomeningitis virus (LCMV) coinfection of C57BL/6 mice led to substantial accumulation of gamma interferon (IFN-γ)-producing LCMV-specific T cells in liver granulomas and increased local IFN-γ. Despite traffic of activated T cells that resulted in a CD8 T-cell-dominated granuloma, the BCG liver organ load was unaltered from control levels. In OT-1 T-cell-receptor (TCR) transgenic mice, ovalbumin (OVA) immunization or LCMV coinfection of BCG-infected mice induced CD8 T-cell-dominated granulomas containing large numbers of non-BCG-specific activated T cells. The higher baseline BCG organ load in this CD8 TCR transgenic animal allowed us to demonstrate that OVA immunization and LCMV coinfection increased anti-BCG protection. The bacterial load remained substantially higher than in mice with a more complete TCR repertoire. Overall, the present study suggests that peripherally activated CD8 T cells can be recruited to chronic inflammatory sites, but their contribution to protective immunity is limited to conditions of underlying immunodeficiency.

Immune responses to chronic infections by intracellular pathogens include delayed-type hypersensitivity reactions such as granulomatous inflammation. Granuloma formation around infected macrophage prevents dissemination of the pathogen and protects surrounding healthy tissue from inflammatory infiltrates. Immunopathologies can arise from long-term deposition of extracellular matrix around the granuloma, leading to fibrosis and organ damage. CD4 T cells are essential for regulating the formation and ongoing function of granulomas induced in response to many infectious agents and, in the absence of these T cells, chronic infectious diseases, including tuberculosis and histoplasmosis, become widely disseminated (6, 29, 36).

Very little research has been directed at understanding what effect, if any, secondary viral infections may have upon granuloma function. Specifically, we questioned what the role of virally activated CD8 T cells might be in augmenting or disrupting granuloma function in the presence or absence of immune deficiency. Over the course of a lifetime, the opportunities for coinfection with *Mycobacterium* and an unrelated viral infection are quite widespread (14). We used a mycobacterial model of *Mycobacterium bovis* strain bacille Calmette-Guérin (BCG) intraperitoneal (i.p.) infection of C57BL/6 mice to model chronic granuloma formation in the liver. At a stage when the infection is chronic, the mice were coinfected with lymphocytic choriomeningitis virus (LCMV) strain Armstrong to induce a dramatic virus-specific immune response. Our studies were designed to answer three questions. Do CD8 T cells induced by viral infection or systemic immunization gain access to BCG-induced granulomas? Does viral infection interfere with granulomatous protection against chronic BCG infection and lead to reactivation of disease? If activated CD8 T cells have access to BCG-induced granulomas, do they provide better protection against BCG or interfere with anti-BCG protective responses? Our data describe a significant accumulation of LCMV-specific gamma interferon (IFN-γ)-producing CD8 T cells in coinfected liver granulomas, but without accompanying augmentation or diminution of protective function in immunocompetent hosts, and with limited protection in immunodeficient ones. These results are discussed in relation to both antigen-specific and non-antigen-specific requirements for T-cell function in granuloma formation.

* Corresponding author. Mailing address: Rm. 5468 MSC, Department of Pathology and Laboratory Medicine, 1300 University Ave., Madison, WI 53706. Phone: (608)265-8715. Fax: (608)262-0846. E-mail: msandor@wisc.edu.

† Present address: Children's Hospital of Wisconsin, Milwaukee, WI.

‡ Present address: Center for Neurologic Diseases, Brigham and Women's Hospital, 77 Avenue Louis Pasteur, HIM 785, Boston, MA 02115-5817.

▽ Published ahead of print on 18 December 2006.

MATERIALS AND METHODS

Animals. In these studies we used C57BL/6 mice (Jackson Laboratories, Bar Harbor, MN) and a T-cell-receptor (TCR) transgenic strain, OT-1, specific for ovalbumin (OVA) SIINFEKL (OVA257-264) peptide in association with major histocompatibility complex (MHC) class I H-2K^b (a gift from K. Hogquist, University of Minnesota at Minneapolis). For adoptive transfer, we used P14 TCR-transgenic mice expressing a Vα2/Vβ8.1 heterodimer specific for LCMV glycoprotein peptide (gp) p33 (KAVYNFATM) and H-2D^b (37) on a CD45.1

background. Animals were housed in animal facilities at the UW Medical School that has AAALAC accreditation and meets Public Health Service requirements. All experiments involving mice were reviewed and approved by the appropriate institutional review committees.

***Mycobacterium* infections.** BCG (substrain Pasteur; Staten Serum Institute) was grown in Middlebrook 7H9 (Difco Laboratories, Detroit, MI)–0.05% Tween 80 with 10% oleic acid dextrose catalase (OADC; Difco) supplement and stored in frozen aliquots at −70°C. For infections, ampoules were thawed, and the inoculum was diluted in saline plus 0.05% Tween 80 and briefly exposed to sonic oscillation in order to obtain a single cell suspension. Mice were infected by i.p. injection with 10^7 BCG in 100 μl (18) in order to maximize the production of liver granulomas. The dose injected is not lethal and induces a disease that is partially cleared with time. Infection was verified by histology of liver tissue samples.

Coinfections with LCMV and VV-ova. LCMV-Armstrong (1) was used in these studies. Five weeks after BCG infection, C57BL/6 or OT-1 mice were infected with LCMV (2×10^5 PFU/mouse i.p.). Nine days later, mice were sacrificed, and their organs were isolated for study by histology and flow cytometry. Vaccinia virus-ova (VV-ova) (39) infection of C57BL/6 or OT-1 mice was initiated 5 weeks by i.p. injection of 10^6 PFU/mouse. These infections were analyzed 7 days after VV-ova infection.

Histology. Small pieces of liver were fixed in 10% formalin prior to being embedded in paraffin for thin sectioning (8 to 10 μm). Hematoxylin and eosin (H&E) staining and Ziehl-Neelsen staining for acid-fast bacteria were done by the UW Department of Pathology's Histopathology Service.

Organ load. Bacterial colony formation was determined by plating serial dilutions of liver homogenates on Middlebrook 7H10 agar plates (Difco) supplemented with 10% OADC and 10 μg of cycloheximide/ml. Colonies were counted after 3 weeks incubation at 37°C. The data are presented as individual mouse values after a $\log_{10}$ transformation. Analysis of variance (ANOVA) was used to determine statistical significance.

Flow cytometry and antibodies. Isolation of bulk granulomas and splenocytes has been described previously (16, 32, 41). Briefly, four livers were homogenized with a tissue blender, and liver granulomas allowed to settle by virtue of their higher density. After the supernatant was decanted, settled granulomas were washed in RPMI 1640. The granuloma pellet was digested with 5 mg of type I collagenase (catalog no. 0130; Sigma Chemical Co., St. Louis, MO)/ml at 37°C for 40 min with shaking. Granulomas were disrupted by using a syringe, followed by removal of any tissue debris by filtration through gauze layers and washing in RPMI. The live leukocyte count was determined by trypan blue staining. Splenocytes or granuloma cell suspensions were incubated for 30 min at 4°C with different labeled antibodies at saturation and then washed and analyzed. Unlabeled 2.4G2 anti-Fc receptor antibody (50 μg/ml) was used to block the binding of labeled antibodies to Fc receptors. Cell surface staining on 10 to 20,000 events was measured by using a FACSCalibur flow cytometer (BD Biosciences, San Jose, CA), and data were analyzed by using either CellQuest (Macintosh version 3.0; BD Biosciences) or FlowJo (Macintosh version 6.2.1; TreeStar, Ashland, OR) software. Fluorochrome-labeled antibodies were purchased from Pharmingen (San Diego, CA) or Sigma (St. Louis, MO).

The construction of the MHCI D^b tetramers that contain the LCMV epitope peptides nucleoprotein 396 to 404 (np396-404) or gp33-41 has been described previously (34). OVA SIINFEKL peptide-specific MHCI K^b tetramers were purchased from Beckman Coulter (Fullerton, CA). For the detection of LCMV-specific or SIINFEKL-specific CD8 T cells, single cell suspensions from spleens or granulomas were surface stained with anti-CD8 antibodies and fluorochrome-labeled MHC I tetramer for 1 h at 4°C, followed by four-color flow cytometry.

Flow cytometric detection of intracellular IFN-γ, TNF, and activated caspase 3. Single cell suspensions of spleen or granuloma cells were cultured in cRPMI 1640 to 10% fetal bovine serum plus a 1:1,000 dilution of Golgistop (Pharmingen). Cells were activated with either 5 μg/ml of anti-CD3 antibody (145-2C11) or 0.2 μg/ml of LCMV np396-404 peptide for 4 to 6 h at 37°C, 5% CO_2. Cells were washed once with fluorescence-activated cell sorting (FACS) staining buffer and surface stained for 30 min at 4°C with the indicated antibodies. After a washing step, the cells were permeabilized for 20 min at room temperature in Cytofix/Cytoperm (Pharmingen), followed by three washes with FACS staining buffer plus 0.1% saponin and staining with either 4 μg/ml of anti-IFN-γ, 4 μg/ml of anti-TNF, or a 1:10 dilution of fluorescein isothiocyanate (FITC)-conjugated rabbit anti-caspase 3 (catalog no. 559341) (Pharmingen) and unlabeled 2.4G2 at 4°C for 30 min. Cells were then washed three times with FACS staining buffer plus+ 0.1% saponin, fixed, and analyzed by four-color flow cytometry. For the measurement of intracellular IFN-γ produced in response to mycobacterial purified protein derivative (PPD), the Golgistop addition was delayed for 12 h to allow processing of the complex protein mixture. Subsequent steps were the same as described above.

Measurement of secreted cytokines. Samples for cytokine analysis were collected from 10^6 liver granuloma cells or spleen cells (live by trypan blue exclusion), seeded into 96-well plates in 0.2 ml of cRPMI, and stimulated with 5 μg/ml of αCD3 antibody. After 72 h, cell culture supernatants were harvested and stored at −70°C until testing. Enzyme-linked immunosorbent assay (ELISA) measurement of secreted IFN-γ was previously described (23). Measurement of secreted TNF used matched reagents from Pharmingen adapted to fluorescence detection according to the instructions of the manufacturer. All data are expressed as the amount of secreted cytokine per 10^6 cells. Confirmatory data was obtained as a custom multiplex cytokine analysis from Linco Research (St. Charles, MO).

Real-time PCR. Total RNA was isolated from 10^6 splenocytes or granuloma infiltrating cells by using TRIzol (Invitrogen, Carlsbad, CA) according to the manufacturer's instructions. cDNA was prepared by using MMLV reverse transcriptase (Gibco-BRL, Gaithersburg, MD) and used as a template for real-time quantitative PCR using primers for IFN-γ and TNF (Biosource International, Camarillo, CA) and β-actin (19). Amplification of primer specific products by a Cepheid Smart Cycler (Sunnyvale, CA) was detected using SYBR green I fluorescence (Molecular Probes, Eugene, OR). The relative signal intensities for cytokines and β-actin were calculated by the comparative C_T (cycle threshold) method using a dilution series of a strongly positive cDNA and reported as an adjusted cytokine level by dividing each cytokine value by the β-actin value for the same sample.

Immunofluorescence. C57BL/6 ($CD45.2^+$) BCG-infected mice were intravenously transferred with 200,000 LCMV-specific P14 transgenic ($CD45.1^+$) T cells prior to LCMV superinfection. Nine days later, mice were perfused with phosphate-buffered saline (PBS) under deep anesthesia. Liver sections were postfixed overnight in 25% sucrose–3% paraformaldehyde in PBS before freezing in Tissue-Tek OCT compound (Sakura Finetek, Torrance, CA) on dry ice. Sections (5 μm) were costained with antibodies to CD8-allophycocyanin (APC) and CD45.1-FITC (1:200 in PBS–1% bovine serum albumin) and imaged with a Bio-Rad MRC 1024 confocal laser scanning microscope (Bio-Rad, Hercules, CA) at ×400 magnification. Digital data were exported into Adobe Photoshop (version 8.0) for further analysis and presentation. Staining with CD8-APC and CD45.1-FITC allowed us to visualize the accumulation of double positive cells within the granulomatous lesions after LCMV superinfection. For staining with LCMV np396-specific MHC I tetramer, livers were harvested from BCG and BCG+LCMV-infected mice as described above without transfer of P14 T cells. Frozen sections were costained with LCMV np396-specific MHC I tetramer-APC and CD8b-FITC (1:100 and 1:50, respectively, in PBS) to visualize accumulation of double-positive cells within granulomatous lesions.

RESULTS

Virus-activated CD8 T cells accumulate in BCG-induced granulomas. To address the question of whether CD8 T cells activated by viral infection have access to BCG-induced granulomas, we coinfected mice with 2×10^5 PFU of LCMV or 10^6 PFU of VV-ova i.p. at 5 weeks after infection with BCG. At this stage BCG infection is chronic and granuloma formation is well established. Mice were sacrificed 9 days after LCMV infection or 7 days after VV-ova infection to study the composition and phenotype of granuloma infiltrating cells. Granuloma cell preparations are made free of contaminating liver parenchymal cells in order to exclusively study cells at the inflammatory site. Seven days is ample time for T-cell homing since granuloma formation can be initiated de novo after 1 week in an adoptive transfer model (23) and is past the peak of both LCMV-specific and VV-ova specific T-cell accumulation in the spleen (5, 39). Figure 1A shows the staining patterns of splenocytes from naive C57BL/6 mice for comparison. In BCG-infected mice the CD8/CD4 T-cell ratio was 1:2 in splenocytes and close to 1:1 in granuloma infiltrating cells in agreement with previous experiments by ourselves and others (Fig. 1B, left-hand panels; see also reference 23). On the ninth day after LCMV coinfection, the ratio of CD8 to CD4 T

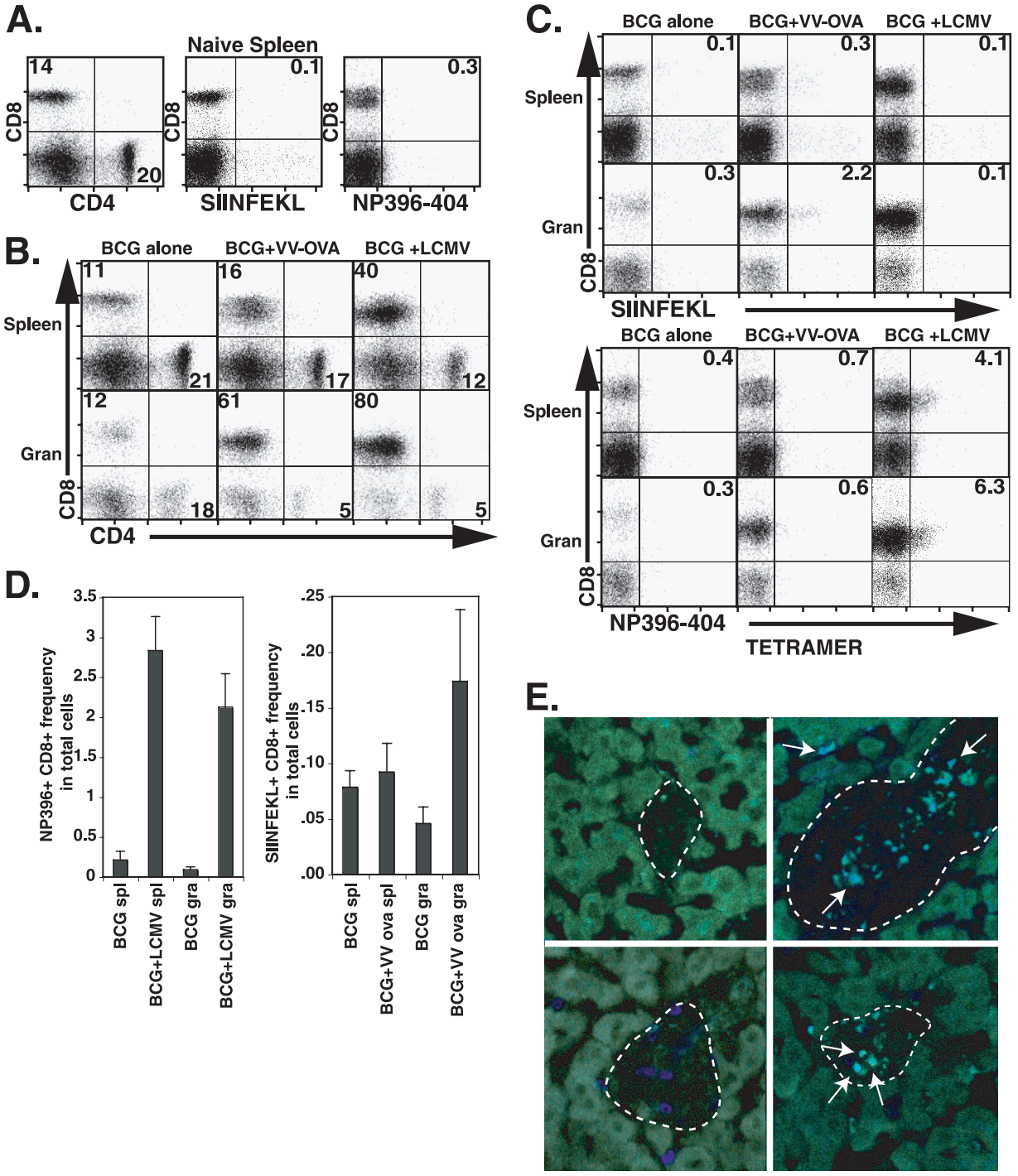

FIG. 1. LCMV-specific T cells can be found in BCG-induced chronic granulomas 9 days after acute LCMV coinfection. C57BL/6 mice were infected i.p. with BCG. At 5 weeks, groups were either held as control infections or coinfected with 2×10^5 PFU LCMV strain Armstrong. VV-ova-coinfected mice received 10^6 PFU at 5 weeks. At 6 weeks of BCG infection, 9 days after LCMV coinfection, or 7 days after VV-ova coinfection, mice were euthanized, and their organs were removed for analysis by flow cytometry. (A) Flow cytometric analysis of splenocytes isolated from naive C57BL/6 mice for comparison. (B) Dot plots show lymphocyte-gated anti-CD4 and anti-CD8 antibody surface staining on splenocytes and granuloma infiltrating cells from the indicated groups. The numbers represent the fractions of the gated populations shown in boxes. (C) Dot plots show lymphocyte-gated anti-CD8 antibody and specific tetramer reagent surface staining on splenocytes and granuloma infiltrating cells from the indicated test groups. The numbers represent the fractions of the gated populations present in the upper right-hand quadrant. The tetramer reagents used included SIINFEKL (MHC-I H-2 K^b/OVA257-264) (top) and np396-404 (MHC-I H-2 D^b/LCMV np396-404) (bottom). Each group was composed of three to four mice. The experiment shown is representative of six with similar results. (D) Mean data are presented for the frequency in the total cell population of LCMV np396-404 tetramer$^+$ CD8$^+$ (left) and OVA SIINFEKL tetramer$^+$ CD8$^+$ (right) cells in the indicated preparations. Error bars represent the SEM. (E) Confocal images at ×400 magnification from LCMV-superinfected BCG-infected liver granuloma (right panels) and BCG-infected liver granuloma (left panels) are shown. The top row stainings show CD8-specific (FITC green) and LCMV np396 tetramer-specific (APC blue) T cells in the liver granuloma 9 days after LCMV coinfection. The bottom row stainings show CD8-specific (APC blue) and CD45.1-specific (FITC green) T cells in the liver granuloma 9 days after P14 cell transfer and LCMV coinfection. Arrows point to double-positive cells, indicating the accumulation of LCMV-specific cells. Liver autofluorescence was used to outline the lesion edges (dotted lines).

cells was 3:1 in the spleen, and CD8 T cells were dominant among granuloma infiltrating cells (16:1; Fig. 1B, right-hand panels). Directly addressing our question, staining with LCMV epitope-specific MHC I tetramer showed that both LCMV np396-404- and LCMV gp33-41 (data not shown)-specific T cells expanded in the spleen as expected and, importantly, both populations were present in a larger proportion among granuloma infiltrating cells. For class I D^b/np396-404 tetramer-positive $CD8^+$ cells, the relative fractions averaged 4.9% ± 0.6% versus 7.2% ± 0.8% ($P \leq 0.01$ [ANOVA]) of gated lymphocytes in the spleen and granuloma, respectively (Fig. 1C, right plots, bottom panels) (average ± the standard error of the mean [SEM]; 2.0% ± 0.1% versus 4.4% ± 0.8% in the spleen and granuloma for class I D^b/gp33-41 tetramer plus $CD8^+$ cells; $P \leq 0.001$ [ANOVA]; data not shown). The mean frequency in total cells is shown in Fig. 1D (left). Thus, after LCMV coinfection, the proportion of virus-specific cells accumulated in chronic granulomatous lesions to a greater extent than in the spleen despite the absence of LCMV in the granuloma. To a somewhat lesser extent, VV-ova coinfection of BCG-infected mice also increased the CD8 ratio in the spleen (1:1). A greater increase in the proportion of CD8 T cells was observed in the granuloma (12:1). In addition, OVA-responsive T cells detected by class I K^b/OVA257-264 tetramer were enriched among granuloma infiltrating cells (Fig. 1C) (0.5% ± 0.2% versus 2.3% ± 0.3% of gated lymphocytes in the spleen and granuloma, respectively; $P \leq 0.01$ [ANOVA]). The mean frequency in the total cells of class I K^b/OVA257-264 tetramer-positive CD8 T cells is shown in Fig. 1D (right). Immunofluorescence was also used to demonstrate the accumulation of LCMV-specific T cells in the BCG-induced liver granuloma after LCMV coinfection for 9 days. LCMV-specific np396 MHC tetramer-APC and CD8-FITC were used to costain frozen liver sections. We were able to clearly visualize $CD8^+$ LCMV np396 $tetramer^+$ cells within the granulomatous lesions after LCMV coinfection (Fig. 1E, top right panel). We also used a P14 adoptive transfer model to demonstrate the presence of P14 transgenic T cells specific for LCMV gp33 in the granuloma. C57BL/6 (CD45.2+) BCG-infected mice were transferred with 200,000 LCMV-specific P14 transgenic (CD45.1+) T cells prior to LCMV coinfection. Nine days later, mice were perfused, and liver sections were fixed for preparation of frozen liver sections. Staining with CD8-APC and CD45.1-FITC allowed us to visualize the accumulation of double-positive cells within the granulomatous lesions after LCMV coinfection (Fig. 1E, bottom right panel). These images clearly show the presence of LCMV-specific CD8 T cells in the BCG-induced granuloma after LCMV coinfection and are in complete agreement with our FACS data. Together, these data indicate that virus-activated CD8 T cells can accumulate in BCG-induced liver granulomas.

Virus-specific T cells in the granuloma have a highly activated phenotype. Next, we examined the activation state of the granuloma-infiltrating virus-specific CD8 T cells. Our data showed that almost all of these cells expressed an activated phenotype. Figure 2A shows that after LCMV coinfection, among the CD8-gated granuloma cells, class I D^b/np396-404 tetramer-positive cells were 98% $CD44^+$ and 78% LFA-1^+. Similar data were seen for class I D^b/gp33-41 tetramer-positive cells (data not shown). The mean frequency in total granuloma is shown in Fig. 2C. Thus, LCMV-specific T cells with a highly activated phenotype locate to the site of chronic BCG infection, and the granuloma repertoire reflects the systemic activated T-cell repertoire.

The greater ratio of CD8 to CD4 T cells in the LCMV-coinfected granuloma might result from both increased CD8 T-cell recruitment and/or increased apoptosis of CD4 T cells. Therefore, we compared caspase 3 expression on CD4 T cells found in BCG-induced granulomas and BCG-induced granulomas altered by LCMV coinfection. Our data showed that the increased proportion of CD8 T cells were clearly the result of higher recruitment since we found equivalent levels of caspase 3 expression by granuloma infiltrating CD4 T cells between BCG alone and BCG+LCMV infections (Fig. 2B and D).

The accumulation of LCMV-specific T cells in the granuloma increases IFN-γ cytokine levels but not TNF levels and does not alter the mycobacterial antigen (PPD) response. We examined whether the accumulation of virally activated T cells in the granuloma effected expression of protective Th1 cytokines TNF and IFN-γ. We measured IFN-γ mRNA, secretion, and intracellular levels in the granuloma. Direct ex vivo measurement of IFN-γ mRNA levels from isolated granuloma cells was done by real-time quantitative PCR and normalized to β-actin mRNA levels measured in the same samples. Normalized IFN-γ mRNA levels were twice as high in LCMV-coinfected samples (Fig. 3A, left) in the experiment shown. As a confirmation, we assessed the recall IFN-γ response of isolated cells by measuring the cytokine production using ELISA of supernatants taken from 3-day in vitro cultures of granuloma infiltrating cells. IFN-γ production by unstimulated cells or in response to mycobacterial PPD was essentially unaltered between control BCG-induced granuloma cells and BCG+LCMV granuloma cells, whereas αCD3-elicited production of IFN-γ was eightfold higher by BCG+LCMV granuloma cells (Fig. 3A, right). The greater response to αCD3 by BCG+LCMV cultures was likely the result of the recruited CD8 T cells in the granulomas (Fig. 1C), which was also supported by intracellular IFN-γ staining (see below).

Figure 3B shows that splenocytes isolated from LCMV-coinfected mice and pulsed with LCMV np396-404 peptide had high numbers of CD8 T cells staining positive for intracellular IFN-γ, whereas control spleens had very low numbers to no CD8 IFN-γ positive cells whether stimulated with LCMV np396-404 peptide or left unstimulated. As expected, granuloma infiltrating cells from control BCG-infected mice had a baseline measurement of IFN-γ that was higher than in splenocytes for either unstimulated conditions or for LCMV np396-404 stimulation. Granuloma cells from LCMV-coinfected animals had substantially higher levels of CD8 IFN-γ^+ T cells after LCMV np396-404 stimulation. This indicates that the activated CD8 LCMV tetramer-positive cells that accumulate in BCG-induced granulomas are functioning effector cells that respond specifically to virus epitopes. IFN-γ-specific staining in response to αCD3 stimulation showed that the LCMV np396-404-specific response was approximately one-third of the total CD8 response in LCMV-coinfected splenocytes or granuloma cells, a finding consistent with the immunodominance of this epitope (45).

Interestingly, IFN-γ^+ staining on CD8-negative lymphocytes was also greater in LCMV-coinfected animals (compare con-

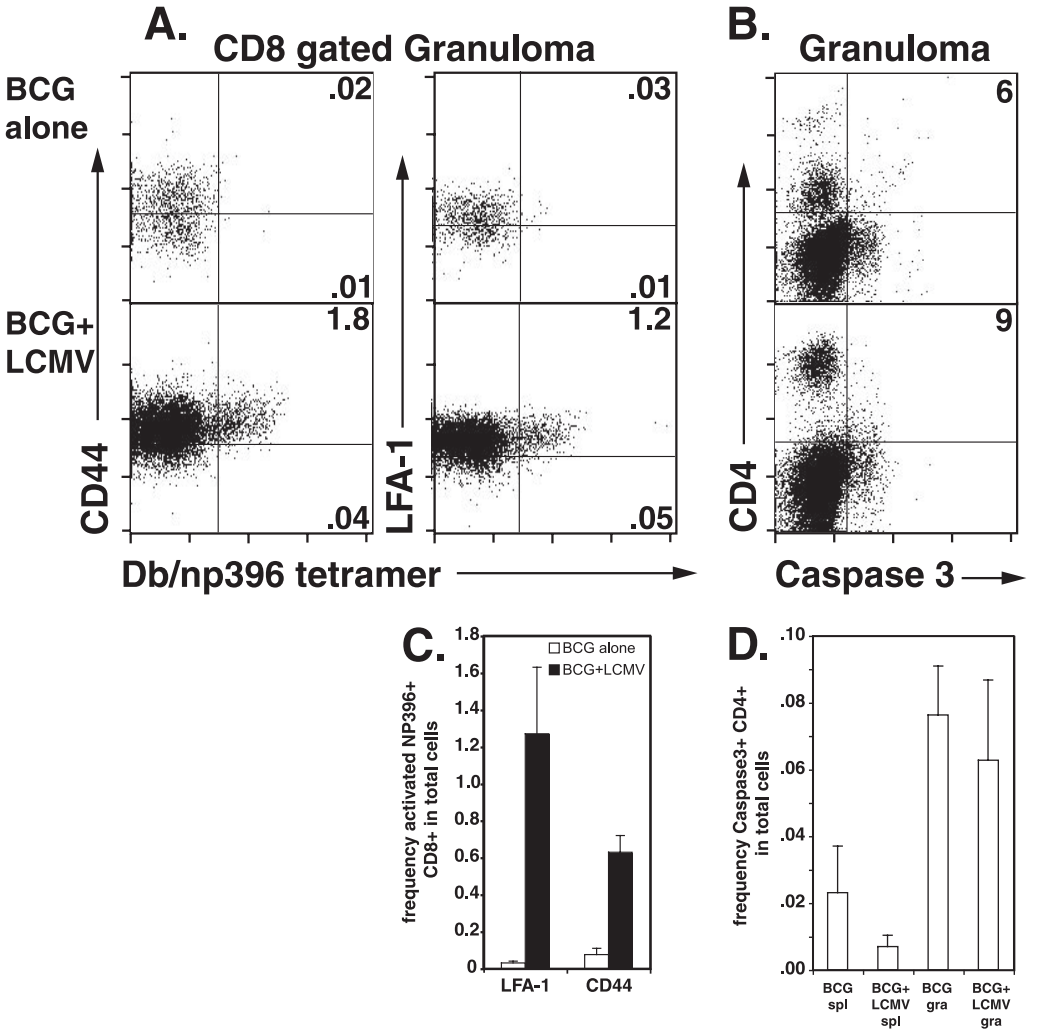

FIG. 2. LCMV coinfection results in the accumulation of a highly activated LCMV-specific CD8 T-cell population in BCG-induced granulomas and has no effect upon activated caspase 3 levels in CD4 T cells. The experimental groups shown are as described in Fig. 1. (A) Dot plots show staining with anti-CD44 (left panels)- or anti-LFA-1 (right panels)-specific antibodies and LCMV np396-404 tetramer on CD8-gated lymphocytes from granuloma infiltrating cells in BCG control infections or BCG+LCMV coinfections of C57BL/6 mice. The numbers shown represent the percentages of total cells contained in the indicated quadrants. (B) Dot plots show staining with anti-CD4 and anti-caspase 3-specific antibodies on lymphocyte-gated granuloma infiltrating cells. The numbers shown represent the $CD4^+$ caspase-3^+ percentage of the total CD4 population. (C) Mean data are presented for the frequency in the total cell population of LCMV NP396-404 $tetramer^+$ $CD8^+$ LFA-1^+ (left) and LCMV np396-404 $tetramer^+$ $CD8^+$ $CD44^+$ (right) cells in the indicated preparations. Error bars represent the SEM. (D) Mean data are presented for the frequency in the total cell population of caspase 3^+ $CD4^+$ cells in the indicated preparations. Error bars represent the SEM.

trol spleen versus LCMV spleen and control granuloma versus LCMV granuloma; bottom row, Fig. 3B, top). Such IFN-γ-producing lymphocytes are likely to be CD4 cells arising in response to LCMV or could represent bystander activation of CD4 T cells reactive to mycobacterial antigens. To distinguish between LCMV-specific and BCG-specific IFN-γ production by granuloma lymphocytes, we measured the intracellular IFN-γ produced in response to mycobacterial PPD under conditions allowing protein processing and presentation since PPD is a complex mixture of proteins. Figure 3C (top panels) shows that CD8 production of IFN-γ did not arise from cells responding to PPD since the CD8 PPD response was no greater than the medium response for both BCG control infection and BCG+LCMV infection. In the control BCG infection, granuloma CD4 T cells responding to PPD with IFN-γ production represented ca. 6 to 7% of the total cells in the lymphocyte gate (5.9% versus 13.1% $CD4^+$ IFN-γ^+ for medium versus PPD responses) (Fig. 3C, bottom panels). αCD3 stimulation did not yield any additional CD4 responsive cells under these conditions. Likewise, in the BCG+LCMV infection, although the baseline of $CD4^+$ IFN-γ^+ T cells was greater (Fig. 3B), the PPD responsive cells constituted ca. 5 to 6% of the total. The balance of the responsive cells in the LCMV coinfection (33.1% responding to αCD3 versus 19.4% to PPD and unstimulated) were most likely responding to LCMV CD4 epitopes (49). While bystander activation of mycobacterial specific T cells cannot be completely excluded in this coinfection model, they probably comprised a small fraction of the total activated T cells in the granuloma. Collectively, the LCMV-coinfected BCG granuloma had a higher

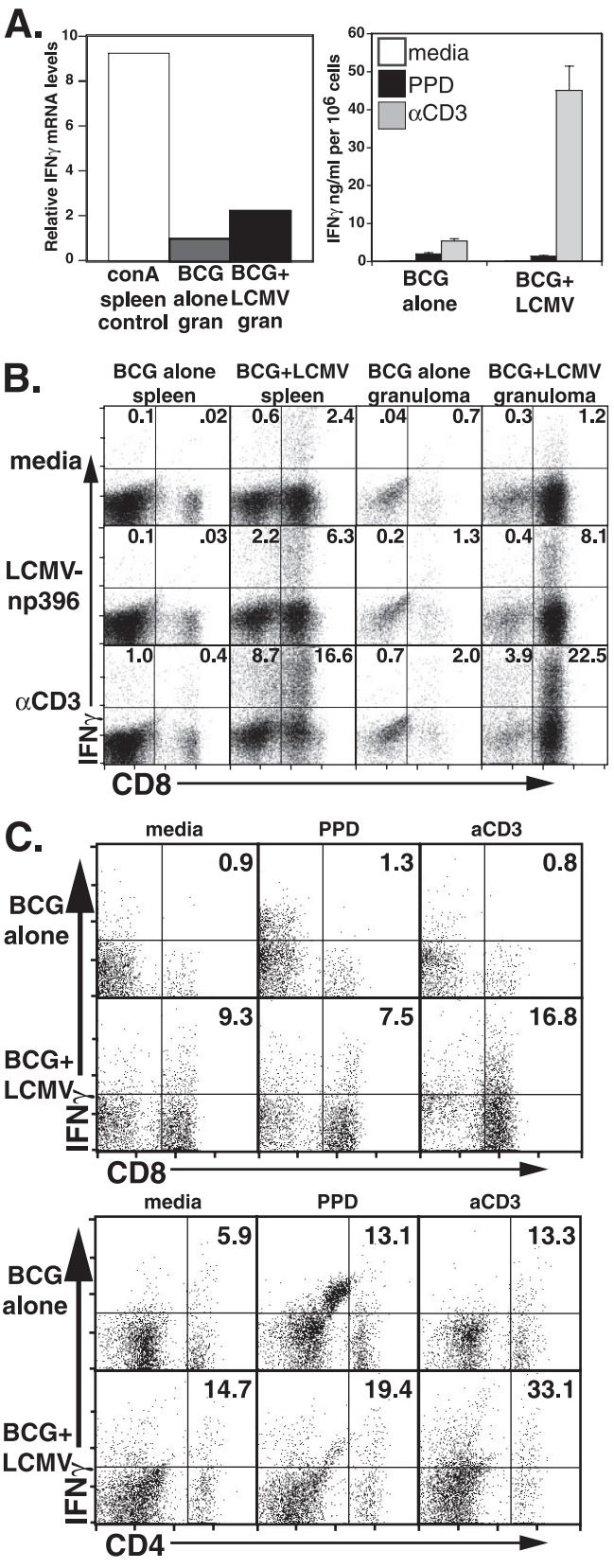

FIG. 3. LCMV coinfection increases IFN-γ mRNA levels. (A) The left-hand panel shows the relative expression level of IFN-γ primer-specific product in cDNAs prepared from granuloma total RNA in one experiment. The value derived from BCG control granuloma was arbitrarily set to 1, and the value for concanavalin A (conA)-stimulated spleen cDNA is included for comparison. The right-hand panel shows the levels of secreted IFN-γ measured by ELISA after 3 days of in vitro culture in media, with mycobacterial PPD antigen, or with 5 μg/ml of αCD3. Error bars represent the SEM. (B) Intracellular staining for IFN-γ was performed on splenocytes and granuloma infiltrating cells from either BCG alone infection or BCG+LCMV coinfection. Cells were cultured for 5 h in the presence of Golgistop in media (top row), with 0.2 μg/ml of LCMV np396-404 peptide (middle row) or with 5 μg/ml of αCD3 (bottom row). Dot plots show anti-CD8 and anti-IFN-γ specific antibody staining on lymphocyte-gated cells from the indicated populations. The numbers are the percentage of gated cells in the quadrants. (C) Intracellular staining for IFN-γ was performed on granuloma infiltrating cells from either BCG alone infection (top rows) or BCG+LCMV infection (bottom rows). Cells were cultured overnight without Golgistop in medium alone (left plots), with mycobacterial PPD (middle plots), or with 5 μg/ml of αCD3 (right plots). After Golgistop addition, the cells were cultured for an additional 4 to 6 h before staining. Dot plots show anti-CD8 (top set) or anti-CD4 (bottom set) and anti-IFN-γ specific antibody staining on lymphocyte gated cells from the indicated populations. The numbers are the percentages of gated cells in quadrants.

level of IFN-γ associated with recruited virus-specific CD8 T cells and a slight increase in CD4 T cells. BCG-specific CD4 T-cell responses were not affected (Fig. 3A and C, bottom plots, middle). Because both the ELISA (Fig. 3, right) and the intracellular staining (Fig. 3B and C) assays depend on reactivation, a more conservative estimate may be in the PCR data, indicating a doubling of the local IFN-γ in the lesions.

Although IFN-γ levels were increased by LCMV coinfection, in vitro TNF production by total granuloma infiltrating cells in response to PPD, LCMV, or αCD3 was not increased as measured by ELISA (Fig. 4A). Likewise, intracellular staining for TNF production following LCMV coinfection of BCG-infected mice was largely unaltered from mice infected with BCG alone (Fig. 4B). We examined whether the large fraction of LCMV-specific CD8 T cells present after LCMV coinfection contributed to TNF production. At day 9 after LCMV infection alone, only a very small population of CD8 cells in the spleen stained with TNF-specific antibodies, even after αCD3 stimulation. This fraction did not appreciably change in BCG-infected spleens or in BCG-induced granuloma infiltrating cells (1.2, 1.5, and 1.7%). Likewise TNF^+ $CD8^-$ cells were present in essentially equal fractions (6.4, 4.9, and 8.4%, respectively) and were not altered by recall challenge with αCD3 (Fig. 4B), PPD, or LCMV (data not shown). Similar data were obtained when intracellular staining was examined for CD4 cell populations (data not shown). Although the fraction of $CD8^-$ cells in total granuloma infiltrating cells that stained with TNF-specific antibodies decreased from 23.6 to 8.4% with LCMV coinfection (Fig. 4B, bottom plots), the TNF-positive proportion of the CD8-negative cells was roughly equivalent. Surface expression of Mac-1 indicated that the major source of TNF in the chronic granuloma was macrophages (data not shown).

Accumulation of virally activated T cells in granuloma does not affect organ load. Microscopic examination of thin liver sections showed that the BCG-induced granulomas found in the control infection remained well-formed after LCMV coinfection (Fig. 5A, top panels). Large numbers of inflammatory

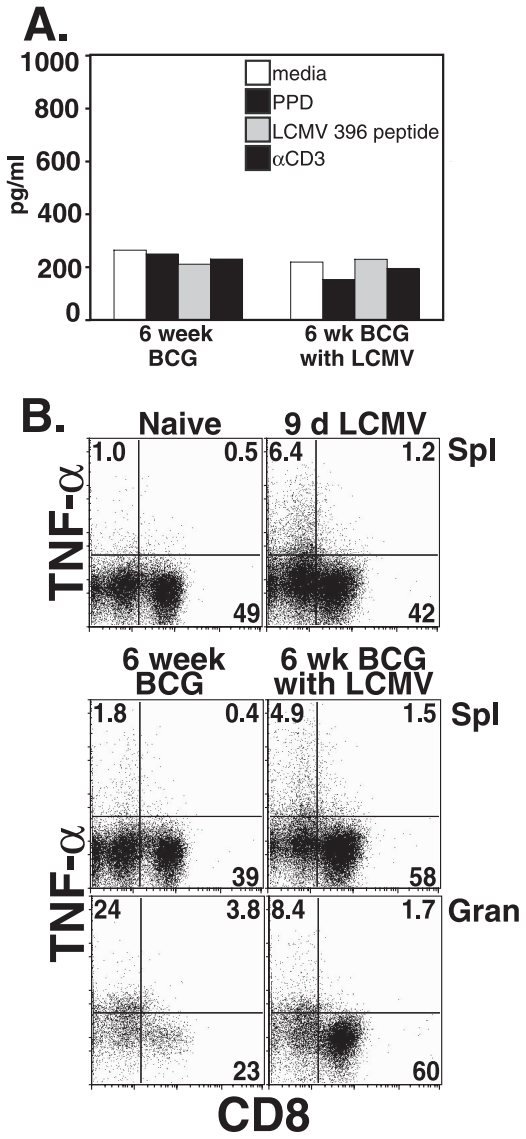

FIG. 4. TNF levels are unchanged by LCMV coinfection. (A) The graph shows the levels of secreted TNF measured by ELISA after 3 day in vitro culture in medium alone, with 5 μl of mycobacterial PPD antigen, with 1 μg/ml of LCMV np396-404 peptide, or with 5 μg/ml of αCD3. The results for one representative experiment of four with similar trends are shown. (B) Intracellular staining for TNF was performed on splenocytes from naive C57BL/6 mice and from mice infected with LCMV virus for 9 days (top, left and right, respectively) and on splenocytes and granuloma infiltrating cells from either BCG alone infection (lower left) or BCG+LCMV infection (lower right). Cells were cultured overnight in 5 μg/ml of anti-CD3, followed by addition of Golgi-stop and an additional 4 to 6 h of incubation before staining for intracellular TNF. Dot plots represent CD8 and TNF specific antibody staining on lymphocyte-gated cells. The numbers are the percentages of gated cells in the quadrants.

cells were also present outside of the liver granulomas, but the number of acid-fast bacilli visible in sections stained by the Ziehl-Neelsen method remained at the low levels characteristic of controlled infections (Fig. 5A, lower panels and data not shown). Plating liver organ homogenates for CFU also showed no difference in organ load between control infections of BCG alone and BCG+LCMV coinfection or BCG+VV-ova coinfection (Fig. 5B). The organ load measured after VV-ova coinfection tended to decrease, but there was no statistical difference between the three groups, and this finding likely lacks biological significance. These experiments established that CD8 T cells activated by LCMV or VV-ova are recruited to the granuloma and are able to enhance the production of protective IFN-γ and yet have no fundamental effect upon protection against BCG in this short-term interval.

SIINFEKL-specific activated CD8 T cells accumulate in BCG-induced granulomas after OVA antigen activation or LCMV bystander activation. It is possible that increases in protection cannot be detected in animals in which BCG infection is controlled. OVA-specific TCR transgenic OT-1 mice are significantly immunocompromised because of greatly reduced levels of CD4 T cells and nontransgenic CD8 T cells (10). Since preliminary experiments indicated that OVA-specific TCR transgenic OT-1 mice infected with BCG had much poorer protection at 6 weeks, we treated BCG-infected OT-1 mice with either OVA immunization to activate the OT-1 T cells or with LCMV coinfection. Baseline stainings of splenocytes from an uninfected OT-1 mouse are shown in Fig. 6A. Consistent with expression of the OT-1 transgene, the CD8 to CD4 T-cell ratio in control BCG-infected OT-1 mice was greater than during infection of C57BL/6 mice (Fig. 6B, left column). CD8 T cells were also predominant in the granuloma (Fig. 6B, lower left plot). After either OVA immunization or LCMV coinfection of BCG-infected OT-1 mice, CD8 T-cell abundance increased in both the spleen and the granuloma (Fig. 6B, middle and right columns) consistent with our hypothesis that peripherally activated T cells preferentially locate to the granulomatous inflammatory site. Similar data were seen with VV-ova infection (data not shown). The antigen specificity of CD8 T cells accumulating in OT-1 after coinfection was examined using class I K^b/OVA257-264 tetramer and class I D^b/np396-404 tetramer (Fig. 6C). Although OVA immunization increased the total fraction of CD8 T cells in granuloma infiltrating cells compared both to spleen or control granuloma cells, the ratio of transgenic cells to nontransgenic cells in the granuloma was lower. This agrees with previous data from our lab in which we observed that infection of AND mice transgenic for pigeon cytochrome C (PCC)-specific TCR resulted in the accumulation of non-PCC specific CD4 T cells in granuloma infiltrating cells (23). Interestingly, whereas LCMV coinfection of OT-1 mice also altered the CD8/CD4 T-cell ratio and promoted the accumulation of more CD8 T cells in the granuloma, tetramer staining for LCMV np396-404 was negative in both spleen and granuloma cell preparations (Fig. 6C, lower panel). The detection of a $CD8^+$ SIINFEKL-tetramer negative population in the granuloma suggests that an LCMV-specific expansion occurs with an altered immunodominance (Fig. 6C, upper panel, lower right). There was no measurable accumulation of LCMV-specific cells in the spleen either ($CD8^+$ class I K^b/OVA257-264 negative) (Fig. 6C, upper panel, upper right).

The expression of LFA-1 on gated CD8 T cells from the OT-1 infection is shown in Fig. 6D. In all three conditions, class I K^b/OVA257-264 tetramer-specific cells were more activated in the granuloma than in the spleen, suggesting bystander activation during both control BCG infection and

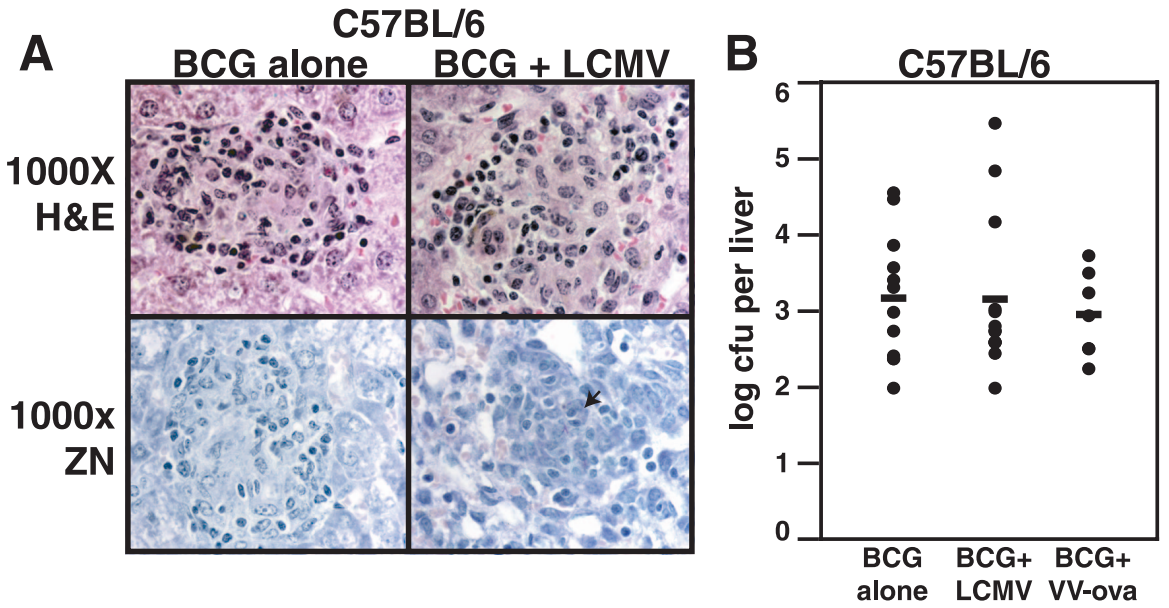

FIG. 5. Acute LCMV coinfection has no significant effect upon antimycobacterial protection in C57BL/6 mice at 6 weeks. (A) H&E-stained (top panels) and Ziehl-Neelsen-stained (bottom panels) thin liver sections from the indicated groups at 6 weeks of infection. Microscopy was at ×1,000 total magnification under oil. The arrowhead in the bottom right panel indicates an individual AFB. (B) Serial dilutions of liver homogenates were plated to determine the CFU/liver after BCG control infection, BCG+LCMV infection, or BCG+VVova infection. Dots represent values for individual mice, and bars represent combined averages for the groups in three separate experiments. No statistical difference was seen between the three groups by ANOVA (n = 12, 13, and 7, respectively).

BCG+LCMV coinfection. Consistent with the C57BL/6 data, the appearance of both LFA-1^+ class I K^b/OVA257-264 tetramer-negative populations (LCMV specific) and LFA-1^+ class I K^b/OVA257-264 tetramer-positive populations (OVA specific) in the BCG-induced granuloma suggests that highly activated, non-BCG specific T cells preferentially accumulate in BCG-induced granulomas in OT-1 mice. The mean frequency in the total cells is shown in Fig. 6E.

Accumulation of SIINFEKL-specific activated CD8 T cells in BCG-induced granulomas decreases BCG load after OVA antigen activation. Equivalent liver granuloma formation in OT-1 mice was observed for BCG infection, BCG+VV-ova coinfection, BCG+LCMV coinfection (Fig. 7A), and BCG+OVA immunization (data not shown). Overall, the bacterial burden in livers from OT-1 infected mice was 3 logs higher than in C57BL/6 mice (Fig. 7B) and closer to values seen in $Rag^{-/-}$ mice (data not shown). Unlike in C57BL/6 mice, in OT-1 mice the liver bacterial burden was improved after viral coinfection (VV-ova or LCMV) or OVA immunization ($\log_{10}$ CFU/liver = 6.4 for BCG control, 5.8 for BCG+OVA immunization, 5.1 for BCG+VV-ova coinfection, and 5.5 for BCG+LCMV coinfection). The higher baseline number of bacteria seen in the OT-1 was likely due to the limited CD4 T-cell repertoire available and the inability of the transgenic and nontransgenic CD8 T cells to provide adequate protective function. Granuloma cells in OT-1 infections produced lower levels of IFN-γ relative to C57BL/6 granuloma cells as measured by ELISA from cell culture supernatants after 3 days of in vitro stimulation with αCD3. Although OVA immunization and LCMV coinfection clearly enhanced the ability of OT-1 splenocytes to produce IFN-γ, IFN-γ-producing cells localizing to the OT-1 granuloma were not sufficiently numerous to reach the level of C57BL/6 granuloma cell IFN-γ production (Fig. 7C, right) or to exert antimycobacterial protection comparable to C57BL/6 (compare Fig. 7B to Fig. 5B). Overall, the 1-log increased protection (Fig. 7B) correlates with increased numbers of CD8 T cells in the granuloma (Fig. 6B) and increased IFN-γ levels (Fig. 7C), underscoring its biological relevance.

DISCUSSION

Granulomatous hypersensitivity lesions are common during the chronic phase of a variety of infectious and autoimmune diseases, and individuals affected with granulomatous diseases are likely to experience concurrent acute viral infections. We were interested in the access of virally activated T cells to granulomatous lesions. Although clearly we must be cautious in generalizing our findings to other granuloma and virus models, our data clearly show that virus-specific CD8 T cells can infiltrate granulomas.

The role of CD4 T cells in antimycobacterial control has long been studied. However, several recent studies have underscored the additional requirement for CD8 T-cell function for control of *M. tuberculosis* infection both during primary immunity after vaccination (12) and during latency (48), and a major pathway of "cross-priming" to MHC-1 and CD1 restricted T cells has been identified (17, 42). Vaccination of mice with a TB DNA vaccine cocktail requires the presence of CD8 T cells for efficacy (12). Antibody depletion studies suggest that primary protective mechanisms induced by the vaccine cocktail involves the induction of activated CD8 cells making cytokines, including IFN-γ and TNF, which can provide antimycobacterial protection in the absence of CD4 T

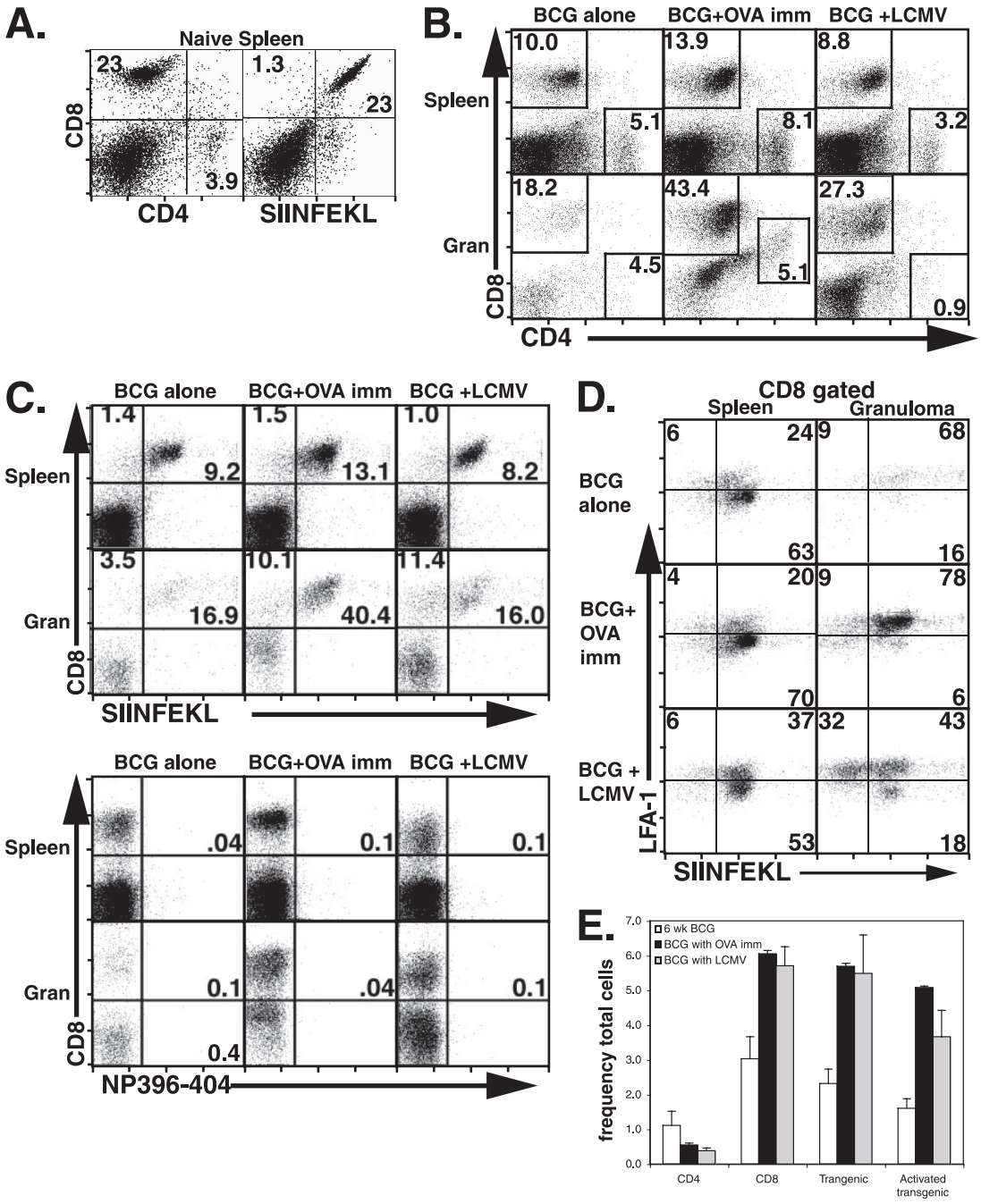

FIG. 6. Enhanced accumulation of activated OVA-specific CD8 T cells can be found in BCG-induced chronic granulomas after OVA immunization of OT-1 mice or after acute LCMV infection of OT-1 mice. OT-1 mice were infected by i.p. injection with BCG. At 5 weeks, groups were either held as control infections, coinfected with 2×10^5 PFU LCMV strain Armstrong, or injected subcutaneously with 100 μg of OVA/CFA. At 6 weeks of BCG infection, 9 days after LCMV coinfection, or 7 days after OVA/CFA immunization, mice were euthanized, and their organs were removed for analysis by flow cytometry. (A) Dot plots show flow cytometric analysis of splenocytes isolated from naive OT-1 mice. (B) Dot plots show lymphocyte-gated anti-CD4 and anti-CD8 antibody surface staining on splenocytes and granuloma infiltrating cells from the indicated test groups. The numbers shown represent the fraction of the gated population shown in boxes. (C) Dot plots show lymphocyte-gated anti-CD8 antibody and specific tetramer surface staining on splenocytes and granuloma infiltrating cells from the indicated test groups. The numbers shown are the fractions of the gated population present in the upper right-hand quadrant. The tetramer reagents used included SIINFEKL (MHC-I H-2 K^b/OVA257-264) and np396-404 (MHC-I H-2 D^b/LCMV np396-404). Each group was composed of two to three mice. The LCMV data are representative of three similar experiments, and results similar to the OVA immunization were found after coinfection at 5 weeks with recombinant VV-ova. (D) Dot plots show staining with anti-LFA-1-specific antibody and SIINFEKL tetramer on CD8-gated lymphocytes from granuloma infiltrating cells in BCG control infections, BCG+LCMV coinfections, or BCG+OVA immunizations of OT-1 mice. The numbers are the percentages of gated cells in the quadrants. (E) Mean data are presented for the frequency in the total cell population of $CD4^+$ (left), $CD8^+$ (center left), LCMV NP396-404 $tetramer^+$ $CD8^+$ (center right), and LCMV np396-404 $tetramer^+$ $CD8^+$ $LFA\text{-}1^+$ (right) cells in the indicated preparations. Error bars represent the SEM.

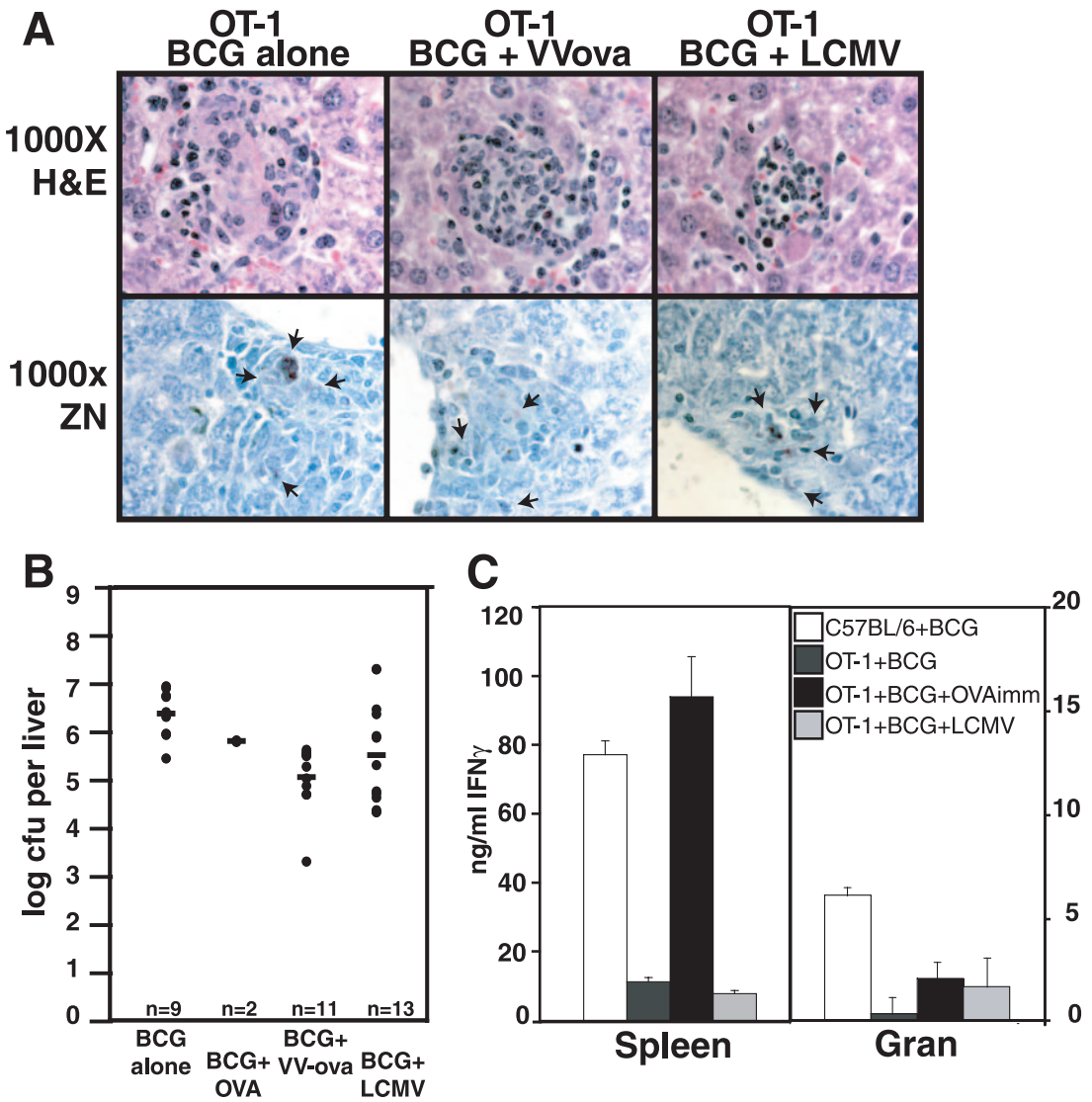

FIG. 7. VV-ova or LCMV coinfection contributes to antimycobacterial protection in OT-1 mice at 6 weeks. (A) Pictures illustrate H&E-stained (top panels) and Ziehl-Neelsen-stained (bottom panels) thin liver sections from the indicated groups of BCG-infected OT-1 mice at 6 weeks of infection. Microscopy was at ×1,000 times total magnification under oil. The arrowheads in the bottom panels indicate AFB. (B) Serial dilutions of liver homogenates were plated to determine the CFU/liver after BCG control infection ($n = 9$), BCG+OVA immunization ($n = 2$), BCG+VV-ova coinfection ($n = 11$), and BCG+LCMV coinfection ($n = 13$) of OT-1 mice. Dots represent values for individual mice, and bars represent combined averages for the groups in three separate experiments. The significance of the decrease in organ load from BCG infection alone was calculated by ANOVA (BCG+VV-ova [$P \leq 0.0001$]; BCG+LCVM [$P < 0.04$]). (C) The graph shows secreted IFN-γ levels measured by ELISA after 3 day in vitro culture with 5 μg/ml of αCD3 for splenocytes (left bars) or granuloma infiltrating cells (right bars) derived from C57BL/6 BCG infection alone, OT-1 BCG infection alone, OT-1 BCG+OVA immunization, and OT-1 BCG+LCMV coinfection. Error bars represent the SEM.

cells. Similarly, depletion of T-cell subsets during latency implicated IFN-γ-producing CD8 T cells in the continued control of bacterial replication at later time points in the lung (48). Given the importance of mycobacterium-specific CD8 T cells to antimycobacterial function, we designed the present study to measure the effect upon bacterial control of the trafficking of non-BCG-specific CD8s induced by nonrelated viral infection. Would virally specific CD8 T cells arrive at the site of mycobacterial infection and, if so, would they diminish or augment bacterial control? Virally induced CD8 T cells might not be appropriately differentiated to act against macrophage infected by mycobacteria. Mouse hepatitis virus infection of the central nervous system suggests that different CD8 T-cell effector mechanisms are responsible for control of coronavirus replication in different central nervous system cell types (4). In contrast, a clinical study associated acute hepatitis B coinfection with the elimination of both hepatitis B and underlying chronic hepatitis C infection, possibly via bystander mechanisms, such as the secretion of cytokines (20). Many virally induced CD8 T cells secrete IFN-γ in large amounts, and this cytokine is key to the control of mycobacterial replication. For the present study, our primary model was LCMV coinfection

of C57BL/6 mice chronically infected with BCG. LCMV coinfections offer the advantage of a superbly characterized infection course and technically advanced analysis reagents.

Our data in Fig. 1 show that CD8 T cells expanded by LCMV infection accumulated in BCG-induced liver granulomas. This was evident from both the frequency of LCMV-specific CD8 T cells among the total population (Fig. 1D) and the calculation of the absolute numbers of T cells present (data not shown). We also demonstrated the accumulation of LCMV-specific cells in the granuloma by immunofluorescence using both LCMV np396-specific tetramer staining and CD45.1 staining of transferred P14 cells (LCMV gp33 specific) (Fig. 1E). While systemically activated CD8 T cells are reported to accumulate in the liver and undergo apoptosis (13), our data show the specific recruitment of activated cells to the granuloma and not the accumulation of apoptotic cells in the liver. In granuloma cells, caspase 3 expression levels were very similar on CD4 T cells from control BCG infection and BCG+LCMV infection (Fig. 2B and D). For CD8 T cells, BCG+LCMV actually had fivefold less caspase 3 staining on a fractional basis than did BCG infection alone due to the accumulation of activated CD8s lacking caspase 3 expression (data not shown). Swain and coworkers found that systemic contraction of BCG-activated CD4 T-cell populations in wild-type mice is associated with increased apoptosis and is dependent upon IFN-γ- and NO-mediated mechanisms (11). Similar mechanisms were found to operate during SEA-induced tolerance of CD4 T cells in TCR transgenic mice (7). This mechanism was not seen despite increases in IFN-γ levels. Figure 2A shows that LCMV-specific T cells that accumulated at the site of chronic BCG infection had a highly activated phenotype. We saw previously that peripherally activated T cells lacking specificity for the inciting pathogen accumulate in liver granulomas (24, 43). Studies in a murine model of virally induced demyelination have also suggested that CD8 T cells lacking specificity for myelin can home to brain inflammatory sites from the periphery and incite neuropathology if specifically activated (21). The CD4/CD8 T-cell ratio in granuloma infiltrating cells is a consistent characteristic that varies between pathogenic agents (22, 23, 41, 51). Our data strongly suggest that the ratio largely reflects systemic activation. It remains to be distinguished whether virus-specific T-cell accumulation in the granuloma reflects a systemic level of activation seen earlier or active accumulation. Mechanisms contributing to accumulation at chronic inflammatory sites are likely to encompass chemokines such as RANTES, MIP-1α, and MCP. Increased levels of these three chemokines, and RANTES most markedly, are produced in vitro by granuloma infiltrating cells in response to LCMV peptide after LCMV coinfection, as assayed by multiplex analysis (data not shown). Enhanced proliferation of LCMV-specific CD8 T cells in the granuloma is unlikely to contribute substantially to their accumulation since granuloma cells are typically in a nonproliferative state and day 9 of superinfection is past the point of LCMV-specific T-cell expansion. We tested our assumption by using flow cytometric intracellular cell cycle analysis and saw no alteration in the extremely low numbers of cells in S phase in BCG+LCMV coinfection compared to BCG-induced granulomas (data not shown).

After either OVA immunization or LCMV coinfection of BCG-infected OT-1 mice, CD8 T cells were more abundant in both the spleen and the granuloma (Fig. 6B). Despite this, although OVA immunization increased the total fraction of CD8 T cells in granulomas compared to spleen and to control granuloma cells, the granuloma ratio of transgenic cells was lower than in the spleen. We previously observed that the infection of AND mice transgenic for a PCC-specific TCR results in preferential accumulation of non-PCC-specific CD4 T cells in granuloma infiltrating cells (23). In both AND and OT-1 mice, when the repertoire is limiting, BCG-specific T cells in the granuloma are preferred, unlike in the C57BL/6, where the initial repertoire is broader. Transgenic OT-1 T cells may also be refractory to normal localization signals. Other studies have demonstrated that transgenic T cells are resistant to a well-characterized inhibitor of T-cell activation, TCDD, when "supraphysiological" numbers of antigen-specific T cells are present in TCR transgenic mice (33).

LCMV coinfection of OT-1 mice alters the CD8/CD4 T-cell ratio and promotes the accumulation of more CD8 T cells in the granuloma, and yet tetramer staining for np396-404 was negative in both spleen and granuloma cell preparations. McGavern et al. found that LCMV infection of OT-1 mice does not lead to any detectable expansion of LCMV peptide-specific IFN-γ production (30), and other reports have detailed altered LCMV immunodominance in genetically deficient mice (45–47). More than 70% of the anti-LCMV response against immunodominant epitopes is reported to come from three distinct TCR populations (44). OT-1 mice may have alterations in the availability of specific Vβ families that abrogate normal immunodominance patterns. Alternatively, BCG infection and/or the extensive TCR transgene expression may bias the ability of dendritic cell populations to present antigen for expansion of the measured LCMV-specific populations. Crowe et al. found that different APC populations are required for the efficient presentation of various immunodominant influenza virus epitopes, leading to changing patterns of immunodominance following primary and secondary infections (9).

The coinfection model with OT-1 mice also demonstrated that highly activated SIINFEKL-specific T cells preferentially accumulated in BCG-induced granuloma versus spleen (Fig. 6D), suggesting bystander activation. Bystander activated OT-1 T cells can modulate the immunopathology of herpes simplex keratitis disease in the absence of herpes simplex virus-specific T-cell reactivity (2). Bystander activation can lead to complex outcomes, including nonreciprocal heterologous immunity (27), bystander recruitment without bystander activation (35), and attrition of bystander CD8 T cells (31). Our experiments in Fig. 6 do not exclude the possibility of dual specificity of the OVA tetramer staining cells arising from imperfect allelic exclusion or low-affinity recognition (3, 28).

It was initially surprising to us that the arrival of activated nonspecific T cells capable of producing IFN-γ did not materially improve or worsen granuloma function in the C57BL/6 model (Fig. 3A and C and Fig. 5). It might be that during chronic-stage infection, after the control of BCG is established, additional effector cells have no effect. Earlier time points might reveal a positive or negative affect of LCMV-activated cells on anti-BCG granuloma function. This suggests that, in the short term, individuals with infectious diseases controlled by granulomatous inflammation can tolerate viral infections

without adverse effect. In the OT-1 model, where baseline liver organ load was 3 logs higher, VV-ova coinfection was able to enhance the control of liver organ load by more than a log, whereas LCMV coinfection led to a somewhat smaller decrease in organ load and had a higher variance. These data support a role for CD8 T cells in protection when CD4 T cells are deficient. Macrophage-tropic LCMV clone 13 variant decreases the response of murine macrophage to IFN-γ in vitro, resulting in the uncontrolled replication of *Histoplasma capsulatum* (50, 52). Double infection with LCMV clone 13 and *H. capsulatum* is also associated with reduced antifungal immunity mediated by CD8 T cells (53). A schistosome LCMV coinfection model demonstrated increased numbers of LCMV-specific CD8 T cells in liver, enhanced hepatotoxicity, and increased morbidity (15). However, other viral studies have strongly suggested that the recruitment of bystander T cells can ameliorate chronic infections (20), and double infections with wild-type LCMV virus and virus expressing altered peptide ligands are less capable of inducing lethal immunopathology (25). Infectious interactions are not always predictable (27), and Jiang et al. found no killing of bystander bacteria when mice containing memory populations of antigen-specific CD8 T cells were infected with mixed inocula of epitope-specific and nonspecific microbes (26). Swain and coworkers have found that influenza infection of the lung gives rise to complex heterogeneous CD4 T-cell responses with a diverse spectrum of effector and memory phenotypes (40). Viral coinfection of the BCG-infected host is no doubt equally multifaceted. Our data show that activated CD8 T cells irrespective of their specificity continuously home to BCG-induced granulomas and may be able to contribute to limited protection in immunodeficient conditions.

An interesting aspect of the unexpectedly high access of virus-activated CD8 T cells in the granuloma concerns the stability and cellular traffic of these sites. Ramakrishnan and coworkers reported that bacterium-infected macrophages have access to well-formed granulomas (8), and here we show that virus-activated CD8 T cells can home to these sites. Previously, we have shown that green fluorescent protein-expressing MOG-specific CD4 T cells (43) and influenza-specific CD4 T cells (7a) home to BCG-induced granulomas (43). Granulomas can be induced in 2 to 3 days (38), but how long they survive and the dynamics of their formation is unknown. The data reported here argue that granulomas are either short-lived and continuously reformed or are dynamically restructured with an active cellular traffic in and out. The implications of a dynamic regenerating granuloma structure are very important for our understanding of the nature of granulomatous diseases.

ACKNOWLEDGMENTS

We thank Khen Macvilay and Shin-Il Kim for assistance with the experiments, Toshi Kinoshita for expert histopathology services, Changying Ling for expert assistance with the confocal microscope, and members of our laboratory for many helpful discussions and criticisms of this work.

This study was supported by National Institutes of Health grants R01AI48087 and R21AI054893 (to M.S.).

REFERENCES

1. **Ahmed, R., A. Salmi, L. D. Butler, J. M. Chiller, and M. B. Oldstone.** 1984. Selection of genetic variants of lymphocytic choriomeningitis virus in spleens of persistently infected mice: role in suppression of cytotoxic T lymphocyte response and viral persistence. J. Exp. Med. **160:**521–540.
2. **Banerjee, K., S. Deshpande, M. Zheng, U. Kumaraguru, S. P. Schoenberger, and B. T. Rouse.** 2002. Herpetic stromal keratitis in the absence of viral antigen recognition. Cell. Immunol. **219:**108–118.
3. **Basu, D., S. Horvath, I. Matsumoto, D. H. Fremont, and P. M. Allen.** 2000. Molecular basis for recognition of an arthritic peptide and a foreign epitope on distinct MHC molecules by a single TCR. J. Immunol. **164:**5788–5796.
4. **Bergmann, C. C., B. Parra, D. R. Hinton, C. Ramakrishna, K. C. Dowdell, and S. A. Stohlman.** 2004. Perforin and gamma interferon-mediated control of coronavirus central nervous system infection by CD8 T cells in the absence of CD4 T cells. J. Virol. **78:**1739–1750.
5. **Butz, E. A., and M. J. Bevan.** 1998. Massive expansion of antigen-specific $CD8^+$ T cells during an acute virus infection. Immunity **8:**167–175.
6. **Cano, M. V., and R. A. Hajjeh.** 2001. The epidemiology of histoplasmosis: a review. Semin. Respir. Infect. **16:**109–118.
7. **Cauley, L. S., E. E. Miller, M. Yen, and S. L. Swain.** 2000. Superantigen-induced CD4 T-cell tolerance mediated by myeloid cells and IFN-gamma. J. Immunol. **165:**6056–6066.

7a. **Co, D. O., L. H. Hogan, J. Karman, E. Heninger, S. Vang, K. Wells, Y. Kawaoka, and M. Sandor.** 2006. Interactions between T cells responding to concurrent mycobacterial and influenza infections. J. Immunol. **177:**8456–8465.

8. **Cosma, C. L., O. Humbert, and L. Ramakrishnan.** 2004. Superinfecting mycobacteria home to established tuberculous granulomas. Nat. Immunol. **5:**828–835.
9. **Crowe, S. R., S. J. Turner, S. C. Miller, A. D. Roberts, R. A. Rappolo, P. C. Doherty, K. H. Ely, and D. L. Woodland.** 2003. Differential antigen presentation regulates the changing patterns of $CD8^+$ T-cell immunodominance in primary and secondary influenza virus infections. J. Exp. Med. **198:**399–410.
10. **Curtsinger, J. M., D. C. Lins, and M. F. Mescher.** 1998. $CD8^+$ memory T cells ($CD44^{high}$, Ly-$6C^+$) are more sensitive than naive cells to ($CD44^{low}$, Ly-$6C^-$) to TCR/CD8 signaling in response to antigen. J. Immunol. **160:**3236–3243.
11. **Dalton, D. K., L. Haynes, C. Q. Chu, S. L. Swain, and S. Wittmer.** 2000. Interferon gamma eliminates responding CD4 T cells during mycobacterial infection by inducing apoptosis of activated CD4 T cells. J. Exp. Med. **192:**117–122.
12. **Derrick, S. C., C. Repique, P. Snoy, A. L. Yang, and S. Morris.** 2004. Immunization with a DNA vaccine cocktail protects mice lacking CD4 cells against an aerogenic infection with *Mycobacterium tuberculosis*. Infect. Immun. **72:**1685–1692.
13. **Dong, H., G. Zhu, K. Tamada, D. B. Flies, J. M. van Deursen, and L. Chen.** 2004. B7–H1 determines accumulation and deletion of intrahepatic $CD8^+$ T lymphocytes. Immunity **20:**327–336.
14. **Dye, C., S. Scheele, P. Dolin, V. Pathania, and M. C. Raviglione.** 1999. Consensus statement. Global burden of tuberculosis: estimated incidence, prevalence, and mortality by country. JAMA **282:**677–686.
15. **Edwards, M. J., O. Buchatska, M. Ashton, M. Montoya, Q. D. Bickle, and P. Borrow.** 2005. Reciprocal immunomodulation in a schistosome and hepatotropic virus coinfection model. J. Immunol. **175:**6275–6285.
16. **Elliot, D. E.** 1996. Methods used to study immunoregulation of schistosome egg granulomas. Methods: Companion Methods Enzymol. **9:**255–267.
17. **Flynn, J. L., and J. Chan.** 2001. Immunology of tuberculosis. Annu. Rev. Immunol. **19:**93–129.
18. **Flynn, J. L., M. M. Goldstein, J. Chan, K. J. Triebold, K. Pfeffer, C. J. Lowenstein, R. Schreiber, T. W. Mak, and B. R. Bloom.** 1995. Tumor necrosis factor-α is required in the protective immune response against *Mycobacterium tuberculosis* in mice. Immunity **2:**561–572.
19. **Giulietti, A., L. Overbergh, D. Valckx, B. Decallonne, R. Bouillon, and C. Mathieu.** 2001. An overview of real-time quantitative PCR: applications to quantify cytokine gene expression. Methods **25:**386–401.
20. **Gruener, N. H., M. C. Jung, A. Ulsenheimer, T. J. Gerlach, H. M. Diepolder, C. A. Schirren, R. Hoffmann, M. Wachtler, M. Backmund, and G. R. Pape.** 2002. Hepatitis C virus eradication associated with hepatitis B virus superinfection and development of a hepatitis B virus specific T-cell response. J. Hepatol. **37:**866–869.
21. **Haring, J. S., L. L. Pewe, and S. Perlman.** 2002. Bystander CD8 T cell-mediated demyelination after viral infection of the central nervous system. J. Immunol. **169:**1550–1555.
22. **Heninger, E., L. H. Hogan, J. Karman, S. Macvilay, B. Hill, J. P. Woods, and M. Sandor.** 2006. Characterization of the *Histoplasma capsulatum*-induced granuloma. J. Immunol. **177:**3303–3313.
23. **Hogan, L. H., K. Macvilay, B. Barger, D. Co, I. Malkovska, G. Fennelly, and M. Sandor.** 2001. *Mycobacterium bovis* strain *Bacillus* Calmette-Guerin-induced liver granulomas contain a diverse TCR repertoire, but a monoclonal T-cell population is sufficient for protective granuloma formation. J. Immunol. **166:**6367–6375.
24. **Hogan, L. H., M. Wang, M. Suresh, D. O. Co, J. V. Weinstock, and M. Sandor.** 2002. $CD4^+$ TCR repertoire heterogeneity in Schistosoma mansoni-induced granulomas. J. Immunol. **169:**6386–6393.
25. **Hunziker, L., M. Recher, A. Ciurea, M. M. Martinic, B. Odermatt, H.**

Hengartner, and R. M. Zinkernagel. 2002. Antagonistic variant virus prevents wild-type virus-induced lethal immunopathology. J. Exp. Med. **196:** 1039–1046.
26. **Jiang, J., L. A. Zenewicz, L. R. San Mateo, L. L. Lau, and H. Shen.** 2003. Activation of antigen-specific CD8 T cells results in minimal killing of bystander bacteria. J. Immunol. **171:**6032–6038.
27. **Kim, S. K., M. A. Brehm, R. M. Welsh, and L. K. Selin.** 2002. Dynamics of memory T-cell proliferation under conditions of heterologous immunity and bystander stimulation. J. Immunol. **169:**90–98.
28. **Kyburz, D., and M. Corr.** 2003. The KRN mouse model of inflammatory arthritis. Springer Semin. Immunopathol. **25:**79–90.
29. **Lawn, S. D., S. T. Butera, and T. M. Shinnick.** 2002. Tuberculosis unleashed: the impact of human immunodeficiency virus infection on the host granulomatous response to *Mycobacterium tuberculosis*. Microbes Infect. **4:**635–646.
30. **McGavern, D. B., and P. Truong.** 2004. Rebuilding an immune-mediated central nervous system disease: weighing the pathogenicity of antigen-specific versus bystander T cells. J. Immunol. **173:**4779–4790.
31. **McNally, J. M., C. C. Zarozinski, M. Y. Lin, M. A. Brehm, H. D. Chen, and R. M. Welsh.** 2001. Attrition of bystander CD8 T cells during virus-induced T-cell and interferon responses. J. Virol. **75:**5965–5976.
32. **Metwali, A., D. Elliott, A. M. Blum, J. Li, M. Sandor, R. G. Lynch, N. Noben-Trauth, and J. V. Weinstock.** 1996. The granulomatous response in murine schistomiasis mansoni does not switch to TH1 in IL-4-deficient C57BL/6 mice. J. Immunol. **157:**4546–4553.
33. **Mitchell, K. A., and B. P. Lawrence.** 2003. T-cell receptor transgenic mice provide novel insights into understanding cellular targets of TCDD: suppression of antibody production, but not the response of $CD8^+$ T cells, during infection with influenza virus. Toxicol. Appl. Pharmacol. **192:**275–286.
34. **Murali-Krishna, K., J. D. Altman, M. Suresh, D. J. Sourdive, A. J. Zajac, J. D. Miller, J. Slansky, and R. Ahmed.** 1998. Counting antigen-specific CD8 T cells: a reevaluation of bystander activation during viral infection. Immunity **8:**177–187.
35. **Ostler, T., H. Pircher, and S. Ehl.** 2003. "Bystander" recruitment of systemic memory T cells delays the immune response to respiratory virus infection. Eur. J. Immunol. **33:**1839–1848.
36. **Perlman, D. C., P. El-Helou, and N. Salomon.** 1999. Tuberculosis in patients with human immunodeficiency virus infection. Semin. Respir. Infect. **14:**344–352.
37. **Pircher, H., K. Burki, R. Lang, H. Hengartner, and R. M. Zinkernagel.** 1989. Tolerance induction in double specific T-cell receptor transgenic mice varies with antigen. Nature **342:**559–561.
38. **Qiu, B., K. A. Frait, F. Reich, E. Komuniecki, and S. W. Chensue.** 2001. Chemokine expression dynamics in mycobacterial (type-1) and schistosomal (type-2) antigen-elicited pulmonary granuloma formation. Am. J. Pathol. **158:**1503–1515.
39. **Restifo, N. P., I. Bacik, K. R. Irvine, J. W. Yewdell, B. J. McCabe, R. W. Anderson, L. C. Eisenlohr, S. A. Rosenberg, and J. R. Bennink.** 1995. Antigen processing in vivo and the elicitation of primary CTL responses. J. Immunol. **154:**4414–4422.
40. **Roman, E., E. Miller, A. Harmsen, J. Wiley, U. H. Von Andrian, G. Huston, and S. L. Swain.** 2002. CD4 effector T-cell subsets in the response to influenza: heterogeneity, migration, and function. J. Exp. Med. **196:**957–968.
41. **Sandor, M., A. I. Sperling, G. A. Cook, J. V. Weinstock, R. G. Lynch, and J. A. Bluestone.** 1995. Two waves of gamma delta T cells expressing different V delta genes are recruited into schistosome-induced liver granulomas. J. Immunol. **155:**275–284.
42. **Schaible, U. E., F. Winau, P. A. Sieling, K. Fischer, H. L. Collins, K. Hagens, R. L. Modlin, V. Brinkmann, and S. H. Kaufmann.** 2003. Apoptosis facilitates antigen presentation to T lymphocytes through MHC-I and CD1 in tuberculosis. Nat. Med. **9:**1039–1046.
43. **Sewell, D. L., E. K. Reinke, D. O. Co, L. H. Hogan, R. B. Fritz, M. Sandor, and Z. Fabry.** 2003. Infection with *Mycobacterium bovis* BCG diverts traffic of myelin oligodendroglial glycoprotein autoantigen-specific T cells away from the central nervous system and ameliorates experimental autoimmune encephalomyelitis. Clin. Diagn. Lab. Immunol. **10:**564–572.
44. **Sourdive, D. J., K. Murali-Krishna, J. D. Altman, A. J. Zajac, J. K. Whitmire, C. Pannetier, P. Kourilsky, B. Evavold, A. Sette, and R. Ahmed.** 1998. Conserved T-cell receptor repertoire in primary and memory CD8 T-cell responses to an acute viral infection. J. Exp. Med. **188:**71–82.
45. **Suresh, M., H. Molina, M. S. Salvato, D. Mastellos, J. D. Lambris, and M. Sandor.** 2003. Complement component 3 is required for optimal expansion of CD8 T cells during a systemic viral infection. J. Immunol. **170:**788–794.
46. **Tewari, K., J. Sacha, X. Gao, and M. Suresh.** 2004. Effect of chronic viral infection on epitope selection, cytokine production, and surface phenotype of CD8 T cells and the role of IFN-gamma receptor in immune regulation. J. Immunol. **172:**1491–1500.
47. **van der Most, R. G., K. Murali-Krishna, J. G. Lanier, E. J. Wherry, M. T. Puglielli, J. N. Blattman, A. Sette, and R. Ahmed.** 2003. Changing immunodominance patterns in antiviral CD8 T-cell responses after loss of epitope presentation or chronic antigenic stimulation. Virology **315:**93–102.
48. **van Pinxteren, L. A., J. P. Cassidy, B. H. Smedegaard, E. M. Agger, and P. Andersen.** 2000. Control of latent *Mycobacterium tuberculosis* infection is dependent on CD8 T cells. Eur. J. Immunol. **30:**3689–3698.
49. **Varga, S. M., and R. M. Welsh.** 1998. Detection of a high frequency of virus-specific $CD4^+$ T cells during acute infection with lymphocytic choriomeningitis virus. J. Immunol. **161:**3215–3218.
50. **Villarete, L., R. de Fries, S. Kolhekar, D. Howard, R. Ahmed, and B. Wu-Hsieh.** 1995. Impaired responsiveness to gamma interferon of macrophages infected with lymphocytic choriomeningitis virus clone 13: susceptibility to histoplasmosis. Infect. Immun. **63:**1468–1472.
51. **Wilson, M. E., and J. V. Weinstock.** 1996. Hepatic granulomas in murine visceral leishmaniasis chagasi. Methods **9:**248.
52. **Wu-Hsieh, B., D. H. Howard, and R. Ahmed.** 1988. Virus-induced immunosuppression: a murine model of susceptibility to opportunistic infection. J. Infect. Dis. **158:**232–235.
53. **Wu-Hsieh, B. A., J. K. Whitmire, R. de Fries, J. S. Lin, M. Matloubian, and R. Ahmed.** 2001. Distinct CD8 T-cell functions mediate susceptibility to histoplasmosis during chronic viral infection. J. Immunol. **167:**4566–4573.

Editor: J. L. Flynn